Radio-frequency discharges in oxygen: III. Comparison of modelling and experiment

2007 J. Phys. D: Appl. Phys. 40 6601

(http://iopscience.iop.org/0022-3727/40/21/020)

IOP Publishing Journal of Physics D: Applied Physics
J. Phys. D: Appl. Phys. **40** (2007) 6601–6607 doi:10.1088/0022-3727/40/21/020

Radio-frequency discharges in oxygen: III. Comparison of modelling and experiment

K Matyash[1], R Schneider[1], K Dittmann[2], J Meichsner[2], F X Bronold[2] and D Tskhakaya[3]

[1] Max-Planck Institut für Plasmaphysik, EURATOM Association, D-17491 Greifswald, Germany
[2] Institut für Physik, Ernst-Moritz-Arndt-Universität Greifswald, D-17489 Greifswald, Germany
[3] Department of Theoretical Physics, Association Euratom-ÖAW, Universität Innsbruck, A-6020 Innsbruck, Austria

E-mail: konstantin.matyash@ipp.mpg.de

Received 26 April 2007, in final form 3 August 2007
Published 19 October 2007
Online at stacks.iop.org/JPhysD/40/6601

Abstract
We present results of 1d3v particle-in-cell Monte Carlo collisions simulations of a capacitive RF discharge in oxygen. Several direct comparisons between experiment and modelling are presented. The calculated ion energy distributions show good agreement with the experimentally measured ones for different discharge parameters. A plausible explanation of a double emissive layer near the powered electrode recently discovered in experiments is suggested. Heavy particle dissociative excitation collisions seem to be responsible for the formation of a second emissive layer close to the electrode. Introducing this process into the simulation a rather good agreement of the simulated axial emission profile with the experimentally observed one can be achieved. This delivers an estimate for the cross section of this collision.

(Some figures in this article are in colour only in the electronic version)

1. Introduction

This is the third paper in a series of combined experimental and modelling studies of RF discharges in oxygen. It concentrates on the direct comparison of the simulation results and experiments, which have been presented before in detail [1, 2].

Capacitive RF discharges are widely used both in laboratory research for production of low-temperature plasmas, and in industry, where they are commonly applied for surface etching and various types of surface modification technologies [3, 4].

For applications of RF discharges detailed information about plasma parameters are necessary. In the case of plasma assisted surface technologies knowledge about the energy distributions of the plasma particles and their fluxes on the substrate is especially important.

Despite the wide application of capacitive RF discharges, a complete quantitative description of such systems is still missing, in particular, with respect to characteristics of energetic particles fluxes, discharge profiles and operation regimes. This is not too surprising, because in such discharges the physics of non-equilibrium non-stationary plasmas is combined with the complexity of reactive plasma processes, including surface interaction, which makes the modeling of such systems quite challenging.

During the last decade the particle-in-cell (PIC) simulation with Monte Carlo collisions (MCC) has established itself as a powerful tool for modelling of capacitive RF discharges, being able to provide insight into discharge dynamics and to deliver plasma parameters which are difficult to measure directly in experiments [5–7].

In this work we present the results of PIC-MCC simulations of capacitive RF discharges in oxygen. Of

particular interest for this system were surface modifications of polymers [8]. Therefore, specific emphasis was put on accurate resolution of charged particles distribution functions and their fluxes to the electrode and we concentrate on the discussion of sheath properties. The sheath determines fluxes and distribution functions of the charged particles at the electrode surface. The recently discovered phenomenon of a double emissive layer in front of the powered electrode [2] is also studied. The simulation offers here a plausible explanation and allows it to verify against the experimental measurements.

2. Experimental setup and the simulation

The details of the experimental apparatus can be found in the second paper of this publication series [2, 8]. It is a parallel plate capacitive RF discharge with stainless steel circular electrodes, 9 cm in diameter and variable spacing d of 1–10 cm. One electrode is grounded and the second is powered from a 13.56 MHz RF voltage source. The amplitude of the driving RF voltage can be varied between 100 and 1000 V (peak to peak). Oxygen is used as a working gas, the gas pressure operation range is 1.5–100 Pa.

For the simulation, we use the PIC-MCC code described in [1, 9]. It resolves one spatial but three velocity components (1d3v). The cross section database for collisions in oxygen plasma was critically assessed and corrected cross sections for elastic scattering (O^-, O_2), recombination (O_2^+, O^-), associative detachment (O^-, O_2) and charge exchange (O_2^+, O_2) were implemented. The resulting code was successfully benchmarked against the measurements of [10]. The details of the code and the discussion of the cross sections can be found in the first paper of this publication series [1].

Although the simulated system is actually three dimensional the discharge behaviour is assumed to be one dimensional along the axis. This is supported by the fact that the electrode diameter is larger than the electrode spacing of $d = 4.5$ cm used in the simulation and that the radial dependence of the plasma parameters close to the symmetry axis can be neglected.

In the simulations, the initial electron density and temperature were chosen as $n_{e0} = 8 \times 10^9\,\mathrm{cm}^{-3}$ and $T_{e0} = 10$ eV, respectively. The computational domain length was $X_{max} = 172\lambda_{D0} = 4.5$ cm. At the positions of the electrodes $X = 0$ and $X = X_{max}$ the absorbing wall boundary conditions were applied. The potential at $X = X_{max}$ was fixed at 0 V, corresponding to the grounded electrode. At the position of the powered electrode at $X = 0$ the potential was assumed to oscillate according to the applied RF voltage: $\varphi(0, t) = U_{RF} \sin(\omega_{RF} t)$ with $\omega_{RF}/2\pi = 13.56$ MHz. Molecular oxygen was used as a background gas. The gas temperature was $T_n = 300$ K, and pressure was varied between 5 and 60 Pa. As the neutral gas density is much higher than the densities of charged species, the neutral gas was treated as a background with fixed density and temperature. Only the dynamics of three charged particles (electrons, O_2^+ and O^- ions) was followed. In order to be able to cope with the rich oxygen plasma-chemistry, a large list of processes was included into the model, representing the most important atom and molecular processes in the oxygen plasma. In total 19 collisional processes are included in the model [1]. A grid size $\Delta x = \lambda_{D0}/2 = 0.013$ cm and time step $\Delta t = 0.2/\omega_{pe0} = 3.965 \times 10^{-11}$ s was used guaranteeing numerical stability. The number of computational particles per Debye length was chosen as $N_d = 2000$, totaling about 10^6 computational particles used in the simulation. The duration of each simulation was of the order of several thousands of RF cycles (millions of time steps) in order to ensure that the system settles to dynamic equilibrium. The calculations were carried out on a single-processor AMD Athlon 2800 GHz+ workstation. The average computational time was about 50 h.

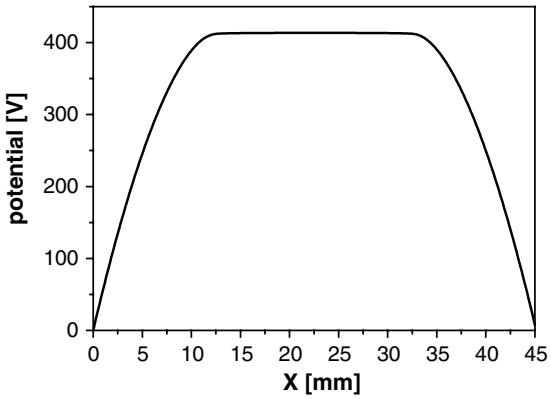

Figure 1. Potential averaged over RF cycle; $p = 5$ Pa, $U_{RF} = 1000$ V.

3. Results and discussion

In figure 1 we present the axial potential profile averaged over the RF cycle for a neutral gas pressure $p = 5$ Pa and a RF voltage amplitude $U_{RF} = 1000$ V. As we can see, a steep potential drop, up to $\Delta\varphi_{max} \approx 413$ V takes place near the electrodes within layers of about $L_s \approx 1$ cm thickness—the RF sheaths. They are created by oscillating positive space-charge layers as discussed in [3]. The electric field in the bulk plasma is negligible in comparison with the field in the sheaths, where it is $\tilde{E}_s \approx 400\,\mathrm{V\,cm}^{-1}$ on average. This strong electric field in the RF sheath regions is directed towards the electrodes, preventing electrons from leaving the plasma for most of the RF cycle. Electrons are able to escape into electrodes only during a short time, when the RF sheath collapses.

In figure 2(*a*) the profile of the distribution function of the axial velocity component for O_2^+ ions averaged over one RF cycle for $p = 5$ Pa and $U_{RF} = 1000$ V is shown. As we can see, in the bulk region the ions are cold, with an average energy close to the thermal energy of the background gas. In the sheath regions, ions are sharply accelerated in the strong electric field towards the electrodes up to the maximum energy of $E_{max} \approx 450$ eV, which is close to the average sheath potential drop. In figure 2(*b*) we plot the averaged ion energy distributions (IEDs) at the powered electrode position for $U_{RF} = 1000$ V and for pressures 5, 10 and 50 Pa. In the low-pressure case (5 Pa) we can distinguish a characteristic saddle-like structure with two peaks in the high-energy part of the IED. This is located around the energy corresponding to the average sheath potential drop $\tilde{U}_s = 413$ V. The time that O_2^+ ions take to traverse the sheath is about $\tau_{O_2^+} \approx 2L_s\sqrt{2e\tilde{U}_s m_{O_2^+}} \approx 451$ ns, while the RF period is $\tau_{RF} = 2\pi/\omega_{RF} = 73.75$ ns. Therefore,

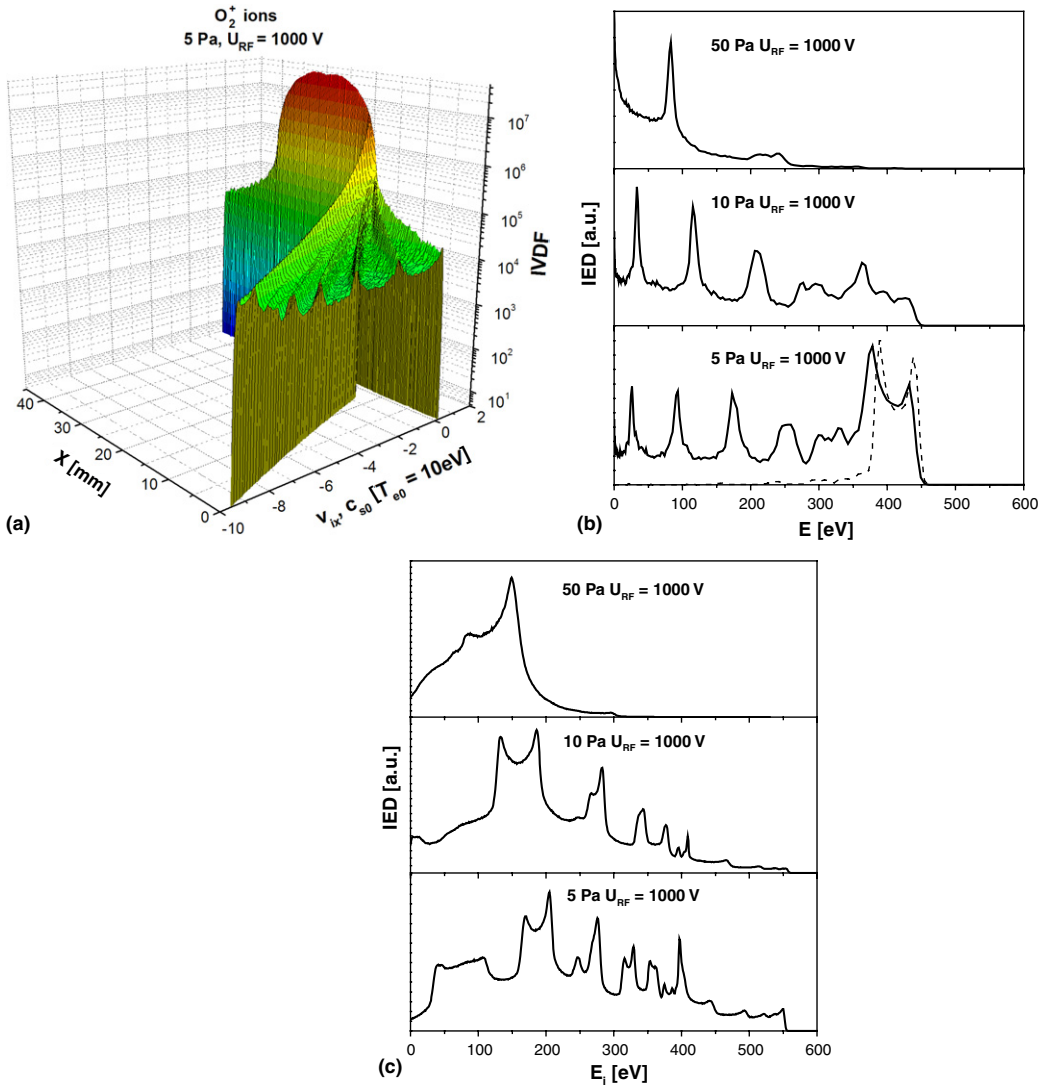

Figure 2. (*a*) O_2^+ velocity distribution and O_2^+ energy distributions at the electrode position (*b*) averaged over RF cycle and (*c*) measured experimentally.

it takes about 6 RF periods for O_2^+ ions to cross the sheath. The ions can only react to the average sheath potential. The saddle-like structure is populated by the ions entering the sheath in a different phase of the RF cycle. They experience a slightly different accelerating potential drop. The continuum and peaks at lower energies in the IED result from ions experiencing elastic and charge-exchange collisions with the neutral gas inside the sheath. During the charge-exchange collision a fast neutral and a slow ion with energy close to the thermal energy of the neutral gas are created. If a collision takes place inside the sheath, these ions experience only a part of the sheath acceleration. The peaks on the top of the continuum in the low-energy part of IED are due to ions created by charge-exchange collisions within the sheath during the time interval when the sheath electric field collapses: $E_s \approx 0$, $\mathrm{d}E_s/\mathrm{d}(\omega_{RF}t) \approx 0$ [11–14]. Thus the number of peaks in the IED is roughly equal to the number of RF periods it takes for the ions to cross the sheath.

In order to distinguish the role of the ion–neutral collisions, we performed the simulation for $p = 5$ Pa and

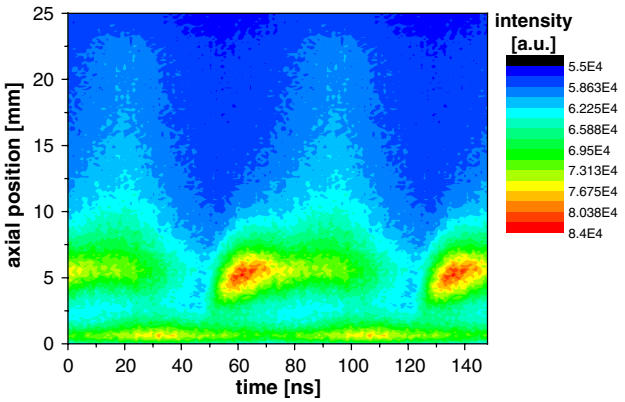

Figure 3. Double emissive layer from experiment (844 nm).

$U_{RF} = 1000$ V in which the ion–neutral elastic and the charge-exchange collisions were switched off. The resulting IED is shown in figure 2(*b*) as a dashed line. As we can see, only the saddle-like structure is pronounced, whereas the low-energy

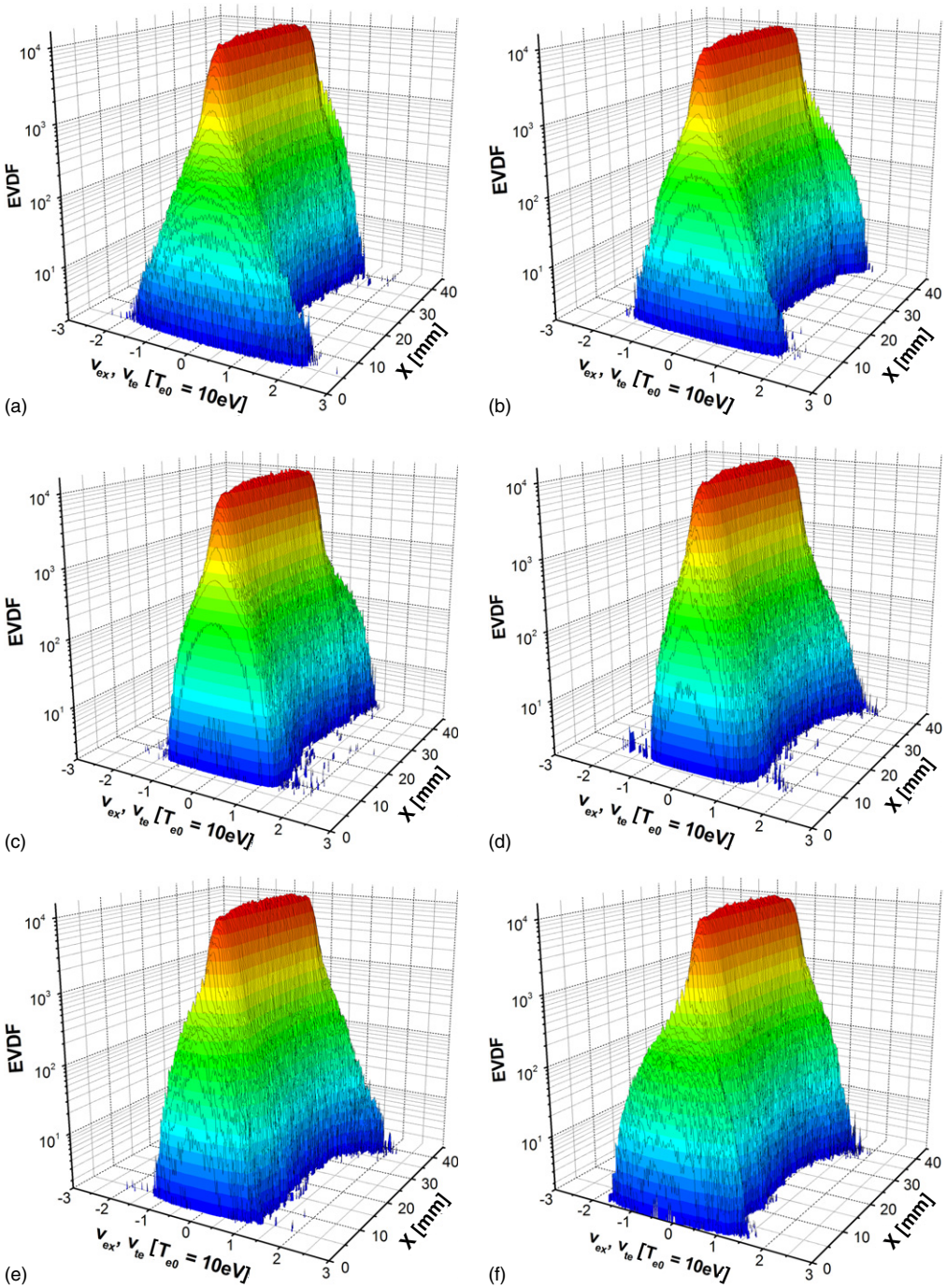

Figure 4. Dynamics of the electron axial velocity component distribution during one RF cycle; $p = 60$ Pa, $U_{RF} = 800$ V. The phase of RF cycle φ is: (*a*) -32.5°, (*b*) 12.5°, (*c*) 57.5°, (*d*) 102.5°, (*e*) 147.5°, (*f*) 192.5°, (*g*) 237.5° and (*h*) 282.5°.

continuum is very weak, because in this case it is populated only by the ions created by electron-impact ionization of the molecular oxygen inside the sheath. As one can see in figure 2(*b*) with an increase in the neutral gas pressure, the ion–neutral collisions in the sheath start to dominate the shape of the IED, depleting the high-energy part and shifting the distribution towards lower energies. In figure 2(*c*) we present the experimentally measured IEDs. As we can see, there is quite good agreement between the simulated and measured IEDs. One should mention that depletion of the sub-100 eV part of the measured IEDs is caused by the limited sensitivity of the ion energy analyzer at this part of the spectrum.

During the experiments in the 20–60 Pa pressure range [2] an interesting phenomenon was observed. The optical light emission at 844 nm from the powered electrode was separated in two layers. The first one, highly modulated with RF frequency layer, was observed about 5 mm from the powered electrode, while the second one, being modulated only slightly was seen almost directly at the powered electrode.

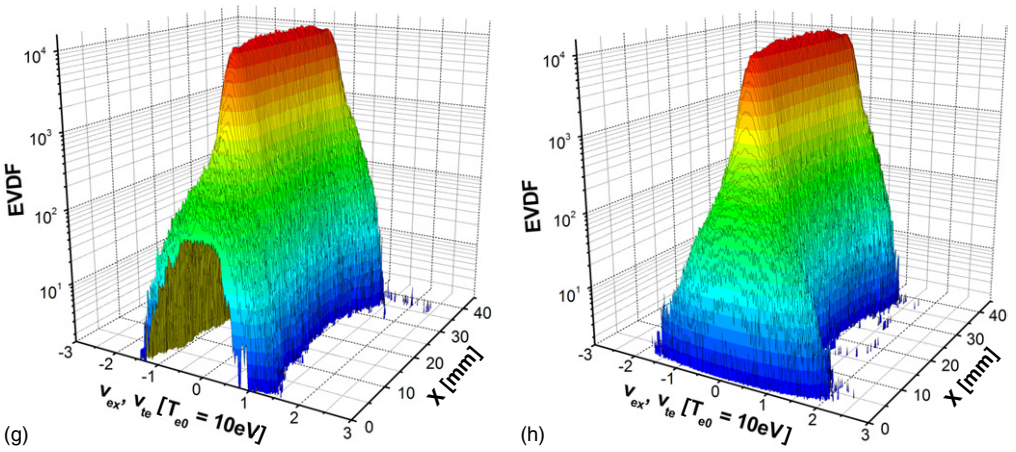

Figure 4. Continued.

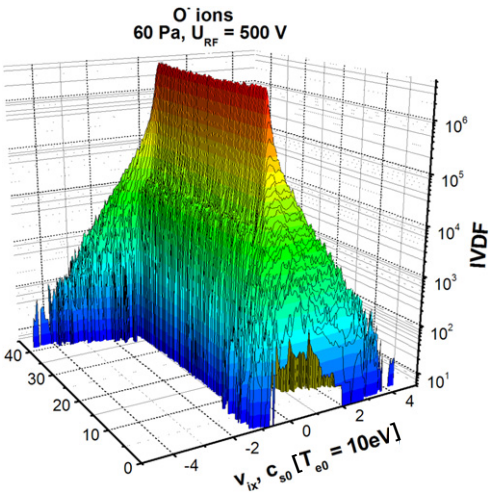

Figure 5. O^- velocity distribution, averaged over RF cycle.

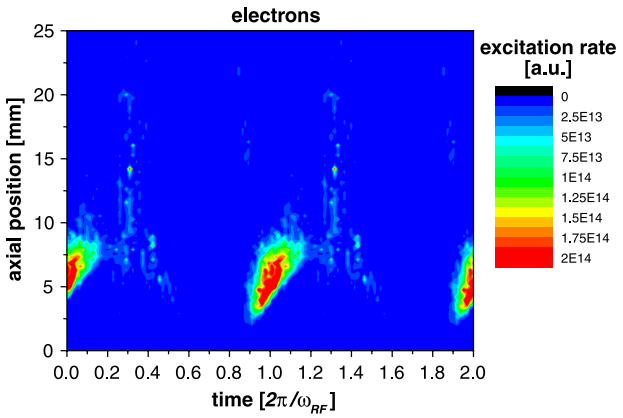

Figure 6. Spatio-temporal distribution of the electron-impact excitation of 844 nm line; $p = 60$ Pa, $U_{\mathrm{RF}} = 800$ V.

In figure 3 we present the spatio-temporal profile of the 844 nm atomic oxygen emission line, corresponding to the $3p^3P \rightarrow 3s^3S$ transition [2]. The origin of the RF modulated optical emission about 5 mm from the electrode is quite clear. This emission is caused by the electron-impact dissociative excitation of the corresponding atomic oxygen levels. Indeed, at these pressures the mean free path of electron–neutral elastic collision becomes smaller than the sheath length, so electrons get their energy in the oscillating sheath electric field between successive elastic collisions with the neutral gas, i.e. Ohmic heating is taking place [3].

In figure 4 we present the eight profiles of the electron axial velocity component distribution from the simulation, corresponding to different phases of the RF cycle. As we can see, high-energy tails in the electron velocity distribution (EVD) are emerging only when the growing sheath is pushing the electrons away from the electrode figures 4(*a*)–(*c*). The electrons reach the maximum energy close to the sheath entrance at about 5 mm from the electrode. These high-energy electrons are responsible for the majority of inelastic electron–neutral processes: ionization, dissociation and excitation.

An additional characteristic of such discharges is the creation of negative oxygen ions. The basic physics of their bulk distribution and the influence of the relevant atomic physics processes are already discussed in the first paper of this series of publications [1]. Here, we concentrate on the discussion of the sheath characteristics. In figure 5 we plot the O^- ions axial component distribution, averaged over the RF cycle for $p = 60$ Pa and $U_{\mathrm{RF}} = 500$ V. We can see that negative ions produced in the sheath are accelerated towards the bulk through the sheath electric field. They reach their maximum energy about 4 mm from the electrode. Further away they are very quickly cooled down to thermal energies of the neutral background gas due to elastic collisions with oxygen molecules. The mean free path for such collisions at 60 Pa is extremely short $\lambda_{\mathrm{O^-O_2el}} \approx 0.4$ mm.

In figure 6 we present the spatio-temporal profile of the electron-impact dissociative excitation of atomic oxygen $3p^3P$ level from the simulation. As one would expect from the electron dynamics, the excitation takes place 3–7 mm away from the electrode during the first quarter of the RF cycle figures 4(*b*) and (*c*). But there is no evidence of an excitation process closer to the electrode as seen in the experiment [2]. This is not really surprising, because, as one can see in figure 4, no energetic electrons are reaching the electrodes. The electrons are able to reach the electrode only during a short time (figure 4(*h*)) to balance the ion current constantly

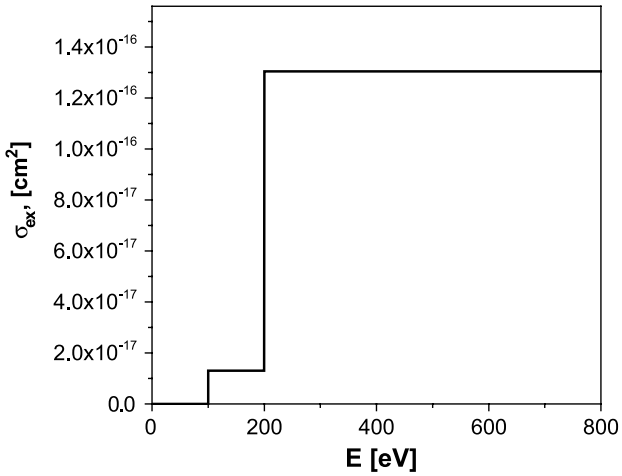

Figure 7. Effective cross section for $O_2^+ + O_2 \rightarrow O(3p^3P) + X$.

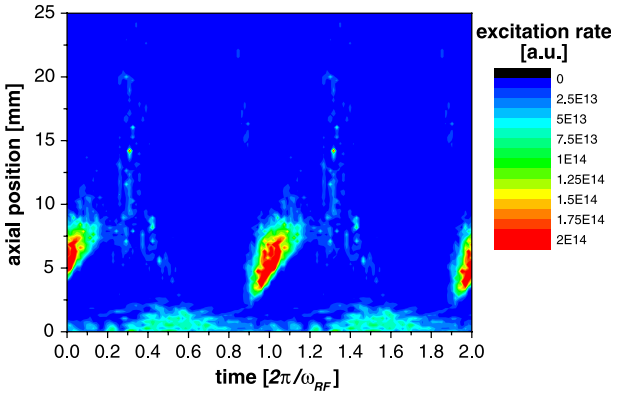

Figure 8. Spatio-temporal distribution of the excitation of 844 nm line; $p = 60$ Pa, $U_{RF} = 800$ V.

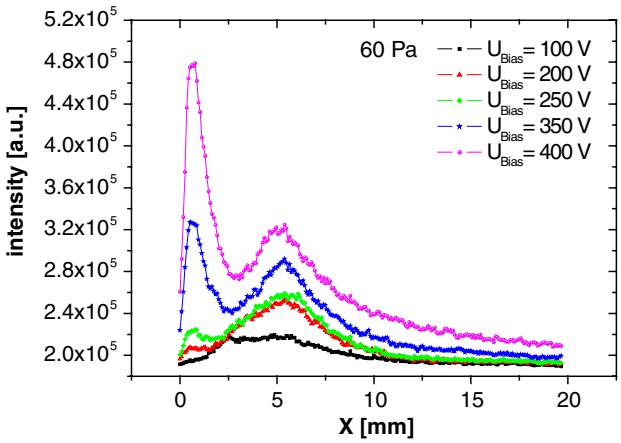

Figure 9. (*a*) RF cycle averaged experimental axial profile of 844 nm emission. (*b*) Total $O(3p^3P)$ excitation rate simulated with PIC.

flowing on the electrode. For the rest of the RF cycle there are no electrons near the electrode. While the energetic electrons are responsible for the RF modulated optical emission (located about 5 mm away from the electrode) the emission layer closer to the electrode needs another explanation.

The dissociative excitation of atomic oxygen by energetic O_2^+ ions is the most plausible channel for this feature. Indeed, the ions get their maximum energy at the electrode, after crossing the sheath. The IED close to the electrode changes only slightly during the RF cycle, because the ions are too heavy to respond to the fast changing sheath electric field.

The only problem is that, to our knowledge, there are no data reported on ion- neutral inelastic collisions in oxygen. We introduced the $O_2^+ + O_2 \rightarrow O(3p^3P) + X$ dissociative excitation process into the model. Here, X expresses the fact that we are summing up all possible production channels of $O(3p^3P)$ excited state. Taking into account that in the experiments the emission from the electrode appears for self-bias voltages higher than 100 V, we set the threshold energy for this process to 100 eV. Starting with a one-step fit the relative height of electron and ion peak for $\tilde{U}_s = 327$ V was reproduced for a value $\sigma_{ex,1} = 1.3 \times 10^{-17}$ cm^2. Analysing the variations of these peaks with RF voltage, a second step was introduced into the cross section (see figure 7) and a reasonable agreement between experiment and modeling was obtained. The energy of the second step was chosen to reproduce strong jump in the intensity of the ion peak at higher RF voltages and a value of $\sigma_{ex,2} = 1.3 \times 10^{-16}$ cm^2 was adopted.

In figure 8 we present the spatio-temporal profile of the dissociative excitation of $O(3p^3P)$, summing up both electron and ion channels. As we can see, the addition of the ion channel resulted in a slightly modulated excitation layer very close to the electrode surface. The overall excitation pattern is very similar to the double layer emission structure from the experiment (figure 3). When comparing the excitation profile from the simulation with the experiment, one should take into account that in the experiment the emission profile is measured. Finite lifetime effects on the excited $O(3p^3P)$ level will lead to formation of a wake-like structure extending the signatures for longer times (as seen in figure 3). In figure 9(*b*) we present the results for the axial profile of the total excitation rate averaged over one RF cycle for different average sheath voltages. Comparing with the experimental measurements [2], presented in figure 9(*a*), one can see rather good agreement.

4. Summary

We applied a newly developed 1d3v PIC-MCC code for simulations of capacitive RF discharges in oxygen. The code includes the corrected cross section database for collisional processes in oxygen [1] and was calibrated against measurements from [10]. In this work the code was able to reproduce the following experimental measurements: the IED functions obtained in the simulation for different pressures are found in good agreement with the measured experimentally. Using the simulation, a plausible explanation of double emissive layer near the powered electrode, recently observed in the experiment [2], was found. The $O_2^+ + O_2 \rightarrow O(3p^3P) + X$ dissociative excitation collisions are the main cause for the emission very close to the electrode. Whereas the emission further away from the electrode is produced due to the electron-impact dissociative excitation by electrons Ohmically heated by the expanding sheath. Using a model cross section for

the ion induced excitation collision we obtain rather good agreement between the simulated and measured emission profiles.

Acknowledgments

Support from the SFB-TR 24 Complex Plasmas is greatly acknowledged. K Matyash and R Schneider acknowledge funding of the work by the Initiative and Networking Fund of the Helmholtz Association.

References

[1] Bronold F X, Matyash K, Tskhakaya D, Schneider R and Fehske H 2007 Radio-frequency discharges in oxygen: I. Modelling *J. Phys. D: Appl. Phys.* **40** 6583 (this issue)

[2] Dittmann K, Drozdov D, Krames B and Meichsner J 2007 Radio-frequency discharges in oxygen: II. Spatio-temporally resolved optical emission pattern *J. Phys. D: Appl. Phys.* **40** 6593 (this issue)

[3] Lieberman M A and Lichtenberg A J 1994 *Principles of Plasma Discharges and Materials Processing* (New York: Wiley)

[4] Raizer Y P, Shneider M N and Yatsenko N A 1995 *Radio-Frequency Capacitive Discharges* (Boca Raton, FL: CRC Press)

[5] Vahedi V, DiPeso G, Birdsall C K, Lieberman M A and Rognlien T D 1993 Capacitive RF discharges modeled by particle-in-cell Monte Carlo simulation: II. Comparisons with laboratory measurements of electron energy distribution functions *Plasma Sources Sci. Technol.* **2** 273

[6] Surendra M, Graves D B and Morey I J 1990 Electron heating in low-pressure rf glow discharges *Appl. Phys. Lett.* **56** 1022

[7] Vender D and Boswell R W 1992 Electron–sheath interaction in capacitive radio-frequency plasmas *J. Vac. Sci. Technol.* A **10** 1331

[8] Meichsner J, Zeuner M, Krames B, Nitschke M, Rochodzki R and Barucki K 1998 Plasma diagnostics for surface modification of polymers *Surf. Coat. Technol.* **98** 1565

[9] Matyash K 2003 Kinetic modeling of multi-component edge plasmas *PhD Thesis* Universität Greifswald, Germany

[10] Katsch H M, Sturm T, Quandt E and Doebele H F 2000 Negative ions and the role of metastable molecules in a capacitively coupled radiofrequency excited discharge in oxygen *Plasma Sources Sci. Technol.* **9** 323

[11] Wild C and Koidl P 1989 Structured ion energy distribution in radio frequency glow-discharge systems *Appl. Phys. Lett.* **54** 505

[12] Wild C and Koidl P 1991 Ion and electron dynamics in the sheath of radio-frequency glow discharges *J. Appl. Phys.* **69** 2909

[13] Fivaz M, Brunner S, Schwarzenbach W, Howling A A and Hollenstein Ch 1995 Reconstruction of the time-averaged sheath potential profile in an argon radiofrequency plasma using the ion energy distribution *Plasma Sources Sci. Technol.* **4** 373

[14] Kawamura E, Vahedi V, Lieberman M A and Birdsall C K 1999 Ion energy distributions in rf sheaths; review, analysis and simulation *Plasma Sources Sci. Technol.* **8** R45